# Chapter 2. Artificial Atoms

**Academic and Research Staff**

Professor Marc A. Kastner, Dr. Olivier Klein

**Visiting Scientists and Research Affiliates**

Theodore M. Lyszczarz,[1] P. Mankiewich,[2] David C. Shaver,[1] Shalom Wind[3]

**Graduate Students**

David Abusch-Magder, David J. Goldhaber-Gordon, Nicole Y. Morgan

## 2.1 Goals and Objectives

### Sponsors

Joint Services Electronics Program
Contract DAAL03-92-C-0001
Grant DAAH04-95-1-0038
National Science Foundation
Grant ECS 92-03427

When electrons are confined to a small particle of metal or a small region of semiconductor, both the energy and charge of the system are quantized. In this way such nanometer-sized systems behave like artificial atoms.[4] The quantization of energy is familiar: The solutions of the Schrodinger equation in an isolated region have discrete energies. In some ways, however, the quantization of charge is more mysterious. We are quite comfortable with the idea that the charge of a collection of electrons is discrete. However, the charge in any small volume of a large sample of conductor is not discrete because the electronic wavefunctions are extended over the entire sample. Only when the states are localized is the charge quantized.

Artificial atoms have been constructed using metals and semiconductors, and they have been given a variety of names: single-electron-tunneling (SET) transistor, quantum dot, single-electron transistor, and zero-dimensional electron gas. The physics of all these devices is the same, although the limits in which they operate may be quite different. The goal of our research is to better understand the physics of these devices in order to optimize their performance so that circuit design may commence.

The kind of artificial atom studied by our group is the single-electron transistor, illustrated in figure 1b.[5] It consists of an inverted heterostructure: a degenerately doped substrate on which is grown a layer of AlGaAs and a layer of undoped GaAs. With source and drain contacts, this corresponds to a standard insulated-gate field-effect transistor. The strong electric field at the AlGaAs/GaAs interface caused by a voltage $V_g$ on the lower gate confines electrons to the lowest quantum level for motion perpendicular to the surface at low temperature T, forming a two-dimensional electron gas (2DEG). The confinement is completed by a set of upper gate electrodes like those illustrated in the figure. In this case the tunnel barriers are introduced by constrictions in the electron channel defined by protrusions of the electrodes. With a lower-gate voltage applied, a droplet of electrons is confined in the potential well between the constrictions.

---

1 MIT Lincoln Laboratory, Lexington, Massachusetts.

2 AT&T Bell Laboratories, Short Hills, New Jersey.

3 IBM Corporation, Thomas J. Watson Research Laboratories, Yorktown Heights, New York.

4 M.A. Kastner, "Artificial Atoms," *Phys. Today* 46(1): 24: (1993).

5 U. Meirav, M.A. Kastner, and S.J. Wind, "Single-Electron Charging and Periodic Conductance Resonances in GaAs Nanostructures," *Phys. Rev. Lett.* 63: 1893 (1990).

## 2.2 Quantization of Energy and Charge

Figure 1a shows the conductance as a function of gate voltage for the single-electron transistor. The conductance is measured by reducing the drain-source voltage to less than kT/e, so that the response is Ohmic. We typically use $V_{ds} \sim 2\mu V$, corresponding to ~ 25 mK, near the base temperature of our dilution refrigerator. Of course, this means that the currents we measure are very small. The noise level seen in figure 1 corresponds to ~ $10^{-15}$ amp. The conductance consists of sharp peaks that are roughly periodic in gate voltage. A calculation of the capacitance between the droplet of electrons and the gate[6] shows that the voltage between adjacent peaks or valleys is that necessary to add one electron to the droplet. At the low temperature of the experiment (electron temperature of ~ 50 mK) the peaks are very sharp so the peak-to-valley conductance ratio is larger than ~ $10^3$ at low gate voltage.

One can understand the periodicity of the conductance peaks using the semiclassical Coulomb blockade model.[7] The classical electrostatic energy stored in placing charge Q on the droplet is

$$E = QV + \frac{Q^2}{2C} \qquad (1)$$

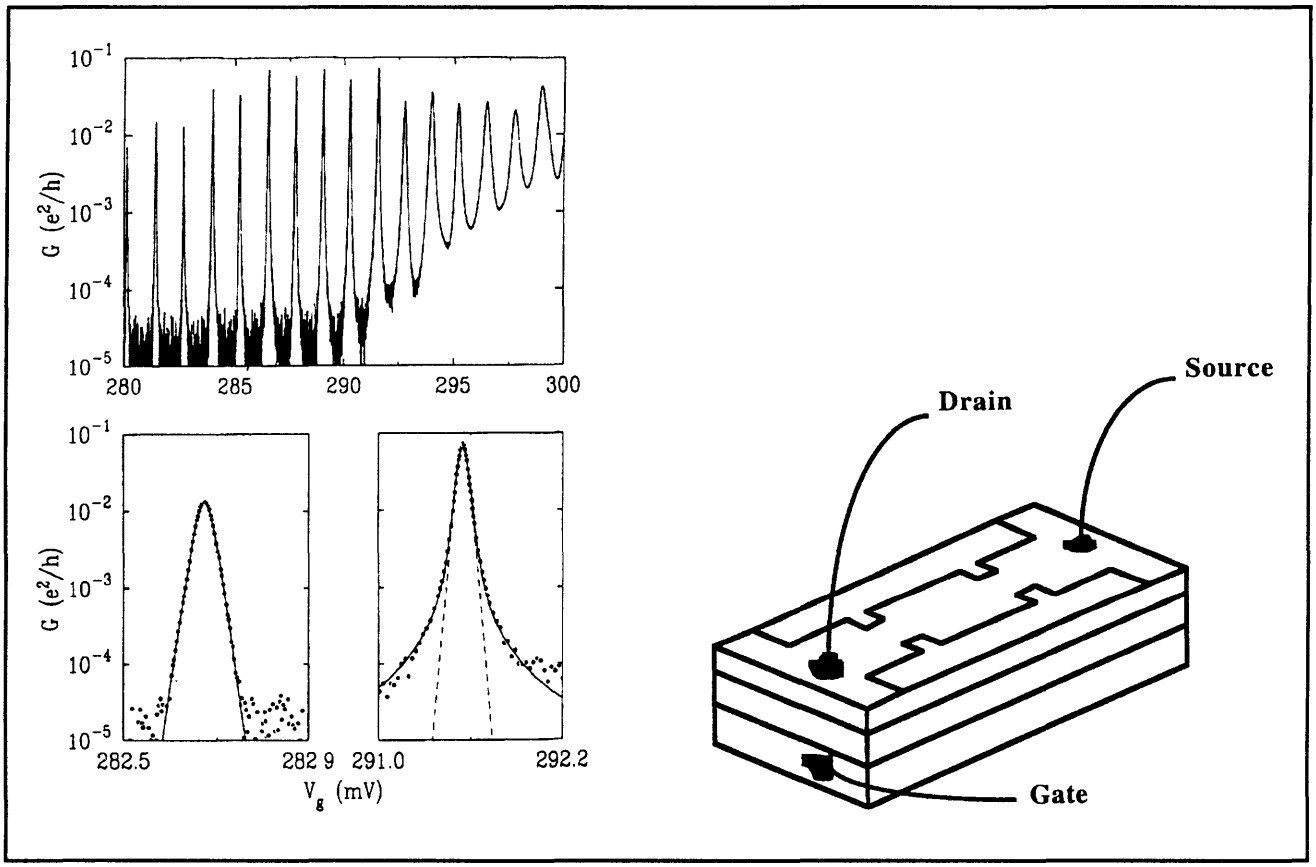


**Figure 1.** (a) Left: Conductance versus $V_g$ showing broadening of levels with increasing $V_g$. Data was taken at magnetic field B = 2.53 T. The alternation of peak heights arises from the two spin states in the lowest Landau level. Bottom: Two of the peaks from the upper panel expanded to better illustrate their shapes. The lower $V_g$ peak is well described by equation (4) and the higher $V_g$ peak displays the Lorentzian tails as predicted by equation (4). (b) Schematic of device structure.

---

6 U. Meirav, M.A. Kastner, and S.J. Wind, "Single-Electron Charging and Periodic Conductance Resonances in GaAs Nanostructures," *Phys. Rev. Lett.* 63: 1893 (1990).

7 D.V. Averin and K.K. Likharev, "Single Electronic Correlated Transfer of Single Electrons and Cooper Pairs in Systems of Small Tunnel Junctions," in *Mesoscopic Phenomena in Solids,* eds. B.L. Altshuler, P.A. Lee, and R.A. Webb (Amsterdam: North-Holland, 1991). This is a comprehensive review of single-electron tunneling in metals.

The first term is the attractive interaction between the droplet and nearby conductors, and the second term is the repulsive interaction among the elements of charge on the droplet. C is the total capacitance of the droplet. If all electrode potentials except that of the gate are held constant, we can write $V = (C_g/C)V_g$ plus a constant. Equation (1) then shows that the energy as a function of Q is a parabola with minimum at $Q_0 = -C_gV_g$ (apart from a constant).

By varying $V_g$, we can choose any value of $Q_0$. However, because the charge is quantized, only discrete values of the energy E are possible. When $Q_0 = -Ne$, for which an integer number N of electrons minimizes E, the Coulomb interaction results in the same energy difference $e^2/2C$ for increasing or decreasing N by one. In other words, there is a gap of size $e^2/2C$ for tunneling onto the artificial atom. For all values of $Q_0$ except $Q_0 = -(N+1/2)e$, the energies for adding or subtracting an electron are not equal, but both are $\geq 0$. The gap is the same size but is shifted relative to the Fermi energy of the leads. Under these circumstances, no current can flow at zero temperature. However, if $Q_0 = -(N+1/2)e$ the state with $Q = -Ne$ and that with $Q = -(N+1)e$ are degenerate; the charge fluctuates between the two values even at zero temperature. Consequently, the energy gap in the tunneling spectrum disappears and current can flow. The peaks in conductance are, therefore, periodic, occurring whenever the average charge on the artificial atom is $Q_0 = -(N+1/2)e$, spaced in gate voltage by $e/C_g$.

## 2.3 Spectroscopy of Artificial Atoms: The Three Energy Scales

The Coulomb blockade model accounts for charge quantization but ignores the quantization of energy resulting from the small size of the artificial atom. The confinement makes the energy spacing of levels in the atom relatively large especially at low energies. One can think of this spacing as roughly $\Delta E = (dN/dE)^{-1}$ where dN/dE is the density of states in the confined region. Because dN/dE increases with energy, $\Delta E$ decreases. If there are many electrons in the atom, they fill up many levels, and the level spacing at the Fermi energy becomes small. The SET transistor has so many electrons that the level spectrum is usually thought of as continuous. However, the underlying discreteness of the level spectrum is essential for the observation of all single-electron phenomena, even those in the SET transistor.

The energy level spectrum can be measured directly by observing the tunneling current at fixed $V_g$ as a function of the voltage ($V_{ds}$) between drain and source. Suppose we adjust $V_g$ so that $Q_0 = -Ne$ and then begin to increase $V_{ds}$. The Fermi level in the source rises in proportion to $V_{ds}$ relative to the drain, so it also rises relative to the energy levels of the artificial atom. Current begins to flow when the Fermi energy of the source is raised just above the first quantized energy level of the atom. As the Fermi energy is raised further, higher energy levels in the atom fall below the Fermi energy, and more current flows because there are additional channels for the electron to use for tunneling onto the artificial atom. Only one electron at a time can enter the atom, but the rate increases because there is more than one channel for the electron to use in tunneling onto the atom. Interestingly, if a level falls below $E_F$ that has a large matrix element for tunneling into the atom but a small one for tunneling out, the current will decrease with increasing $V_{ds}$ giving a negative differential conductance.[8] We measure the energies of the levels by measuring the voltage at which the current increases (or decreases), or, equivalently, the voltage at which there is a peak (or valley) in the derivative of the current $dI/dV_{ds}$. Many beautiful tunneling spectra of this kind have been measured for quantum dots. We show one for our device in figure 2a. Similar level spectra have been reported by several groups.[9]

Increasing the gate voltage lowers all the energy levels in the atom by $-eV_g$, so that the entire tunneling spectrum shifts with $V_g$. This effect can be observed by plotting the values of $V_{ds}$ at which peaks appear in $dI/dV_{ds}$, as is in figure 2b. One can see the gap in the tunneling spectrum shift lower with increasing $V_g$ and then disappear at the charge-degeneracy point, just as predicted by the

---

[8] J. Weis, R.J. Haug, K. von Klitzing, and K. Ploog, "Magnetotransport Investigations of a Quantum Dot with a Small Number of Electrons," *Physica B* 189: 111 (1993).

[9] J. Weis, R.J. Haug, K. von Klitzing, and K. Ploog, "Magnetotransport Investigations of a Quantum Dot with a Small Number of Electrons," *Physica B* 189: 111 (1993); J. Weis, R.J. Haug, K. von Klitzing and K. Ploog, "Competing Channels in Single-Electron Tunneling through a Quantum Dot," *Phys. Rev. Lett.* 71: 4019 (1993); E.B. Foxman, P.L McEuen, U. Meirav, N.S. Wingreen, Y. Meir, P.A. Belk, and S.J. Wind, "Effects of Quantum Levels on Transport Through a Coulomb Island," *Phys. Rev.* B 47: 10020 (1993); A.T. Johnson, L.P. Kouwenhoven, W. de Jong, N.C. van der Vaart, C.J.P.M. Harmans, and C.T. Foxon, "Zero-Dimensional States and Single-Electron Charging in Quantum Dots," *Phys. Rev. Lett.* 69: 1592 (1992).

Coulomb blockade model. One can also see the discrete energy levels of the artificial atom. For the range of $V_{ds}$ shown in figure 2b, the voltage is only large enough to permit one extra electron to tunnel onto the atom. The discrete levels are the excited states of the atom with one extra electron or one extra hole. At still higher voltages (see figure 2c) we observe levels for adding two electrons and so forth. That is, a Coulomb staircase is seen with small steps superposed, corresponding to excited states of the artificial atom. The charge-degeneracy points are the values of $V_g$ for which one of the energy levels of the artificial atom is degenerate with the Fermi energy in the leads when $V_{ds} = 0$, because only then can the charge of the atom fluctuate.

In the SET transistor the energies for adding electrons are equally spaced, by $e^2/C$, because the average electron-electron interaction completely determines the energy. For the quantum dot of Ashoori[10] the energy spacings are large at low voltage, for which there are very few electrons in the artificial atom, but the spacings decrease with increasing number until they become approximately equally spaced. This happens because there is a large quantum mechanical confinement contribution to the energy for adding an electron at low number N of electrons, but the charging energy dominates the addition energy at high N.

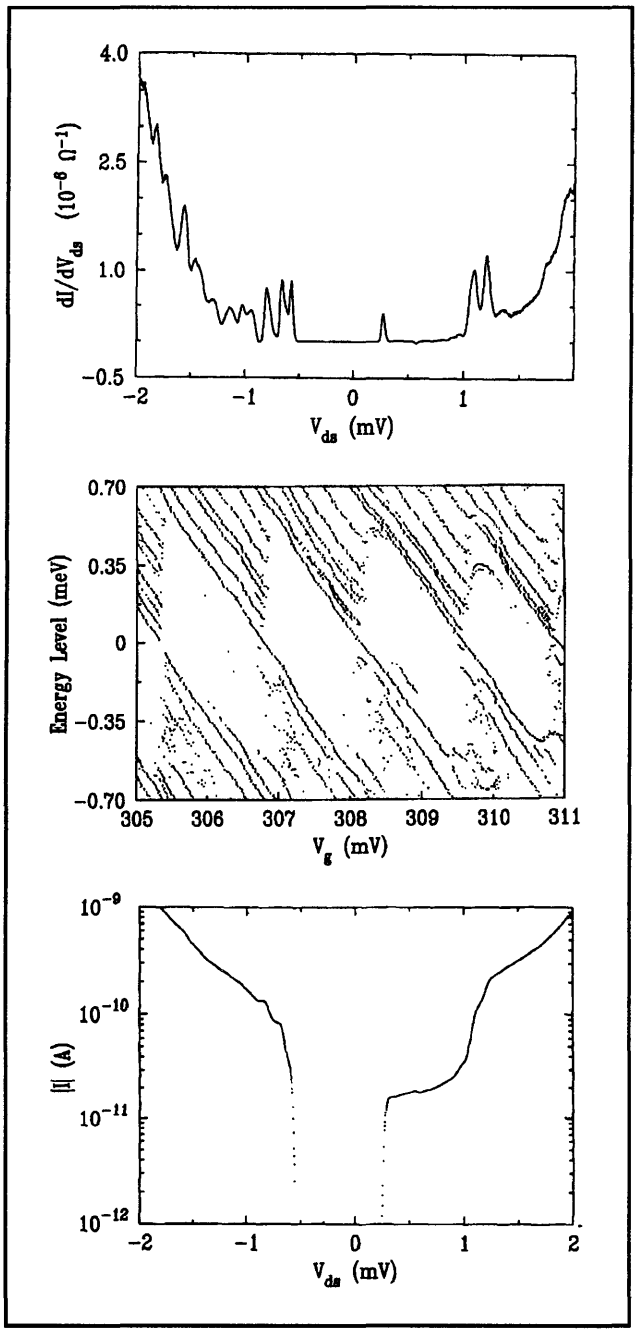


**Figure 2.** (a) Differential conductance at fixed $V_g$. The peaks and valleys correspond to $V_{ds}$ at which the Fermi level in the leads is degenerate with the energy levels of the droplet of electrons. (b) Values of $V_{ds}$ at which peaks and valleys are observed as a function of $V_g$. (c) Current as a function of $V_{ds}$ found from integrating the data in figure 2a.

[10] R.C. Ashoori, H.L. Stormer, J.S. Weiner, L.N. Pfeiffer, S.J. Pearton, K.W. Baldwin, and K.W. West, "Single-Electron Capacitance Spectroscopy of Discrete Quantum Levels," *Phys. Rev. Lett.* 68: 3088 (1992); R.C. Ashoori, H.L. Stormer, J.S. Weiner, L.N. Pfeiffer, S.J. Pearton, K.W. Baldwin, and K.W. West, "N-Electron Ground State Energies of a Quantum Dot in Magnetic Field," *Phys. Rev. Lett.* 71: 613 (1993).

In addition to the Coulomb interaction and the confinement energy, there is a third energy scale that is very important in understanding the behavior of artificial atoms. This is the width $\Gamma$ of the energy levels resulting from tunneling between the artificial atom and the leads. Beenakker[11] suggested that the conductance near the charge degeneracy point should be given by that for resonant tunneling of non-interacting particles even though Coulomb interactions are obviously important. At zero temperature this single level conductance is

$$G_s = p\frac{e^2}{h}\frac{\Gamma_L\Gamma_R}{(E-E_o)^2+\Gamma^2} \qquad (2)$$

Here $\Gamma_L$ and $\Gamma_R$ are the tunneling rates (multiplied by h) through the left and right barriers, respectively, $\Gamma = (\Gamma_L + \Gamma_R)/2$, p is the level degeneracy, E is the energy at which the tunneling occurs, and $E_o$ is the energy of the resonant level. At finite temperature the conductance is given by the convolution of $G_s(E)$ in equation (2) with the negative derivative of the Fermi-Dirac distribution function so the conductance is given by

$$G_s = p\frac{e^2}{h}\pi\frac{\Gamma_L\Gamma_R}{\Gamma^2}\int dE\,\frac{1}{kT}$$

$$\frac{\Gamma^2}{(E-E_o)^2+\Gamma^2}\,\mathrm{sech}^2\left[\frac{E-\mu}{2kT}\right] \qquad (3)$$

where $\mu$ is the chemical potential of the leads. Since the Lorentzian becomes a $\delta$ function in the limit $\Gamma \rightarrow 0$, $G_s$ for narrow resonances is proportional to the derivative of the Fermi-Dirac function $(1/kT)\mathrm{sech}^2[(E-\mu)/2kT]$.

In our experiments, the electrochemical potential difference varies in proportion to the voltage $V_g$ on the lower gate. In the limit $\Gamma << kT$, equation (2) reduces to

$$G_s = p\frac{e^2}{h}\pi\frac{\Gamma_L\Gamma_R}{\Gamma}\frac{1}{2kT}\mathrm{sech}^2\left[\frac{E_o-\alpha eV_g}{2kT}\right] \qquad (4)$$

where we have used $\mu = \alpha eV_g$, and $\alpha = U/e\Delta V_g$ is measured from the T dependence of the peak widths.[12] Meirav et al.[13] showed that equation (4) is in excellent agreement with experimental shapes of conductance peaks at low $V_g$. An illustration of this is shown in the lower left panel of figure 1a. For higher $V_g$, the tails of the Lorentzian become apparent. However, over the entire range of $V_g$, equation (3) describes the conductance peaks very well. (See lower right panel of figure 1a.)

It is clear from this discussion that the tunneling measurements provide a spectroscopy of the energy levels of artificial atoms just as photoelectron spectroscopy provides a spectroscopy of the levels of natural atoms. In the case of tunneling the resolution of the spectroscopy is kT. When $kT < \Gamma$, one can probe the line shape of the levels. When $kT < \Delta E$, one can measure the level spacings. However, when $\Delta E < kT < U$, one can only measure the charging energy. The SET devices made of metals are always in the latter regime because $\Delta E$ and $\Gamma$ are so small, whereas semiconductor devices may operate in any of the three regimes.

## 2.4 Criterion for Single-Electron Effects

It is well known that the condition for observation single-electron phenomena is that the conductance of the tunnel barriers must be less than the quantum of conductance $e^2/h$. However, it is not often made clear what this means on a microscopic level. It is usually argued that this criterion comes from the requirement that the charging time through the tunnel junction $R_TC$ be greater than the uncertainty time given by h/U. With $U = e^2/C$ this gives the correct criterion. However, it gives no insight into the underlying physics. To develop this insight, we must realize that the fundamental criterion for single-electron phenomena is that $\Delta E > \Gamma$. This is obviously the condition under which the energy of the droplet can be considered discrete. However, Thouless[14] pointed out that it is also the condition for localization of charge on the droplet. Only when the charge is localized can there be a Coulomb gap in the tunneling spectrum. Thus single-electron

---

[11] C.W.J. Beenakker, "Theory of Coulomb-Blockade Oscillations in the Conductance of a Quantum," *Phys. Rev. B* 44: 1646 (1991).

[12] E.B. Foxman, P.L McEuen, U. Meirav, N.S. Wingreen, Y. Meir, P.A. Belk, and S.J. Wind, "Effects of Quantum Levels on Transport Through a Coulomb Island," *Phys. Rev.* B 47: 10020 (1993).

[13] U. Meirav, M.A. Kastner, and S.J. Wind, "Single-Electron Charging and Periodic Conductance Resonances in GaAs Nanostructures," *Phys. Rev. Lett.* 63: 1893 (1990).

[14] D.J. Thouless, "Maximum Metallic Resistance in Thin Wires," *Phys. Rev. Lett.* 39: 1167 (1977).

effects can only be seen when $\Delta E > \Gamma$. Following Thouless, the current through the droplet is

$$I = \frac{e}{t}\frac{dN}{dE}eV_{ds} \qquad (5)$$

where t is the time for an electron in a single quantum state to traverse the droplet, and $(dN/dE)eV_{ds}$ is the number of such current-carrying channels. Using $\Gamma = h/t$ and $dN/dE = 1/\Delta E$, we find that the condition $\Delta E > \Gamma$ is the same as $G < e^2/h$.

Foxman et al[12] presented data which demonstrate that the Coulomb charging energy disappears when G exceeds $e^2/h$. Their results are shown in figure 3. Fitting the peaks in the top panel with the form of equation (3) one extracts U and $\Gamma$ for each one. In addition, using the data of figure 2 and similar data taken by reversing the source and drain, one can determine the separate capacitances between the droplet and each lead, $C_r$ and $C_l$. By varying the voltages on the top gates, one observes a sequence of conductance peaks like those in the top panel of figure 3 from which one determines the capacitance between the top gates and the droplet, as well. Adding up all the capacitances, one can compute $e^2/2C$, where C is the total capacitance, and this agrees well with U determined from fitting the peaks with equation (3). One should note that in all these experiments we actually measure current not the charge on the droplet, so we are not actually measuring the capacitances. Instead, we are measuring the changes with voltage of the energy of the droplet relative to the leads.

One sees from figure 3 that U goes to zero at a critical gate voltage $V_c$. This happens because one of the tunnel-barrier capacitances (labeled $C_r$) diverges as $(1-V_g/V_c)^{-1}$. As one approaches $V_c$ from below, $\Gamma$ grows exponentially, as demonstrated in the second panel of figure 3. This is presumably because the tunnel barrier height is lowered by the gate voltage, and $\Gamma$ is an exponential function of this height. In the absence of the magnetic field, one would expect $\ln\Gamma \sim \sqrt{(\phi - \mu)}$ where $\phi$ is the potential energy, but in a strong magnetic field, $\ln\Gamma \sim (\phi - \mu)$, as observed.[15]

Although Foxman et al did not appreciate this at the time of their experiment, it can all be understood in a simple way. As the gate voltage is increased, one of the barriers becomes transparent before the other because they are not identical and because their transmission varies exponentially with $V_g$. The

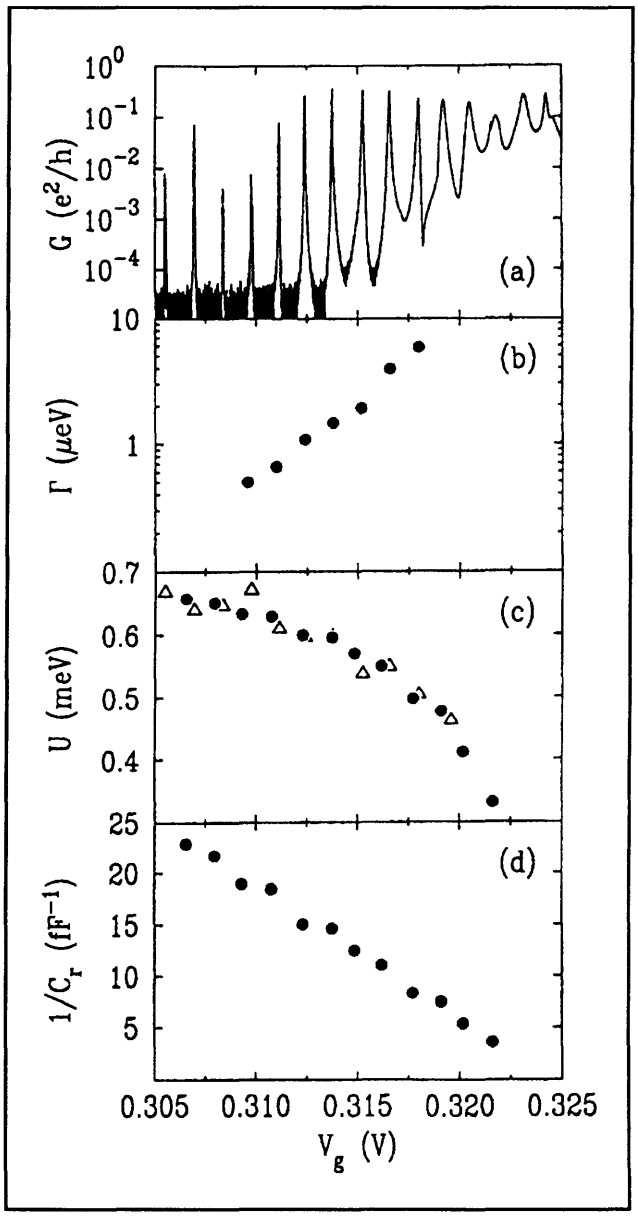


**Figure 3.** (a) Conductance versus gate voltage. (b) Full width at half-maximum of the Lorentzian component in each peak in (a) found by fitting equation (3). (c) Coulomb charging energy U determined (triangles) by fitting each peak with equation (3) using $\mu - \alpha eV_g$ and $\alpha = U/e\Delta V_g$, where $\Delta V_g$ is the spacing between peaks. Also shown is U determined (solid circles) by adding up all capacitances and using $U = e^2/2C$. (d) The reciprocal of the capacitance between the droplet of electrons and one of the leads, arbitrarily labeled the right.

localization length $\lambda$ for the transparent barrier grows as $\sim(\phi - \mu)^{-1}$ and diverges at the critical voltage at which the height of the barrier above the

[15] H.A. Fertig and B.I. Halperin, "Transmission Coefficient of an Electron Through a Saddle-Point Potential in a Magnetic Field," *Phys. Rev.* B 36: 7969 (1987).

Fermi energy goes to zero. The Coulomb energy associated with transfer of electrons across this barrier is $\sim e^2/\lambda$, which goes to zero at the critical gate voltage at which the localization length diverges. For the experiment of figure 3, $V_c$ is about 0.325 V. Extrapolating G to $V_c$, one sees that it reaches ~ 50 eV at the critical point. This is just the average spacing between the levels $\Delta E$ extracted from the data of figure 2.

Thus, theory and experiment are in excellent agreement. The criterion for charge quantization and energy quantization are the same: the level spacing must be larger than the level width. This is true for metallic structures, like the SET transistor, as well. The condition $G < e^2/h$ guarantees that $\Delta E > \Gamma$ even though both quantities are smaller than kT, and therefore cannot be determined.

## 2.5 Crossover from Single to Multilevel Transport

At high enough temperatures, which is always the case for metallic single-electron devices, current is carried by many adjacent levels because $kT > \Delta E$. In this multilevel regime, the conductance is given by Kulik and Shekhter:[16]

$$G_m = \frac{e^2}{h}\frac{\rho}{4}\frac{\Gamma_L\Gamma_R}{\Gamma}\frac{\mu_c - \alpha eV_g}{kT}$$

$$\operatorname{csch}\left[\frac{\mu_c - \alpha eV_g}{kT}\right] \qquad (6)$$

where $\rho$ is the density of levels (i.e., $1/\Delta E$) and $\mu_c$ is the chemical potential for which there is a charge degeneracy point for the artificial atom. That is, $\mu c/\alpha e$ is the gate voltage at which the states with N and N+1 electrons have the same energy, the condition for a conductance peak. To better than one percent, equation (6) is equivalent to

$$G_m = \frac{e^2}{h}\frac{\rho}{4}\frac{\Gamma_L\Gamma_R}{\Gamma}\operatorname{sech}^2\left[\frac{\mu_c - \alpha eV_g}{2.5kT}\right] \qquad (7)$$

which has the same functional form as equation (4) for single level transport. However, the temperature dependencies are different. The peak height for the single level conductance is proportional to 1/T whereas for the multilevel conductance, it is temperature independent. The latter comes about because each level contributes a conductance that decreases as 1/T, but the number of levels contributing increases as T. In addition to this difference in the T dependence of the peak height, the full width at half maximum of the peak is 3.5 kT for the single-level case but is 4.35 kT for the multilevel case.

These effects have been recently seen in our experiments.[17] Figure 4 shows the temperature dependence of a single peak. Figure 4a shows the inverse of its amplitude as a function of T, which is proportional to T at low T as predicted by the single level form (equation 4). Above about 0.5 K the peak conductance becomes independent of temperature as predicted by the multilevel form (equation 6 or 7). The width of the peak also shows this crossover. The full width at half maximum is plotted as a function of T in figure 4b. The shallower line in the lower panel is the single-level prediction, 3.5 kT, and the steeper line is the multilevel prediction, 4.35 kT. This is dramatic evidence for the crossover from single-to-multilevel behavior and shows that the crossover occurs in a narrow range of T. The crossover temperature is expected to be $\sim \Delta E$, which gives $\Delta E \sim 40$ $\mu$eV. This is consistent with the level spacings measured by Foxman et al[18] using source-drain tunneling spectroscopy (figure 2). As mentioned above, the SET devices made of metals are always in the multilevel regime because the level spacings are so small.

---

[16] I.O. Kulik and R.I. Shekhter, "Kinetic Phenomena and Charge Discreteness Effects in Granulated Media," *Zh. Eksp. Teor. Fiz.* 68: 308 (1975), *Sov. Phys.-JETP* 41: 308 (1975).

[17] E.B. Foxman, U. Meirav, P.L. McEuen, M.A. Kastner, O. Klein, P.A. Belk, D.M. Abusch, and S.J. Wind, "Crossover from Single-level to Multilevel Transport in Artificial Atoms," *Phys. Rev. B.* 50: 14193 (1994).

[18] E.B. Foxman, P.L McEuen, U. Meirav, N.S. Wingreen, Y. Meir, P.A. Belk, and S.J. Wind, "Effects of Quantum Levels on Transport Through a Coulomb Island," *Phys. Rev.* B 47: 10020 (1993).

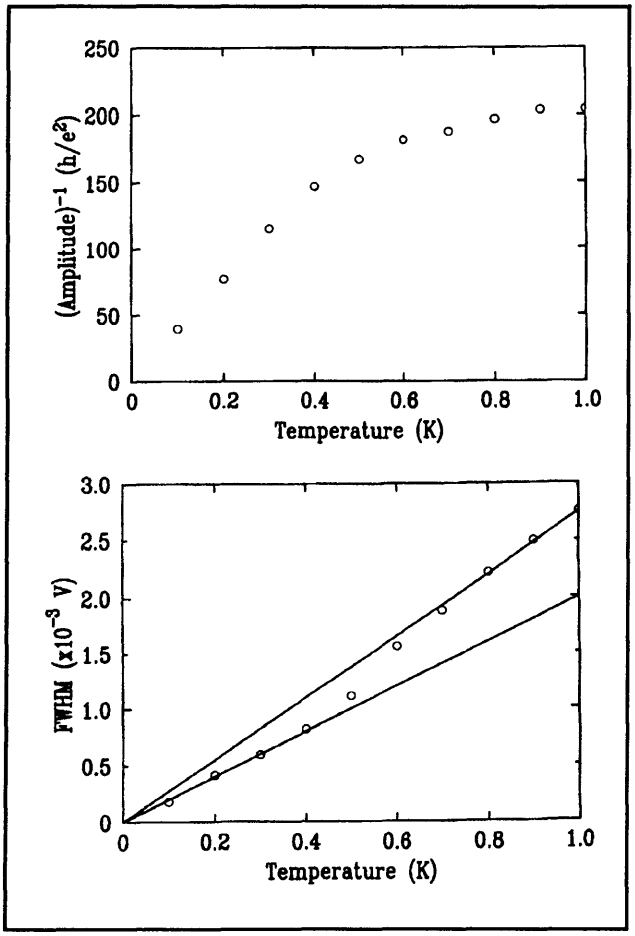


**Figure 4.** (a) Top: Height of one conductance peak as a function of temperature. The $T^{-1}$ dependence indicates single-level transport. At higher T the conductance becomes constant indicative of multilevel transport. The crossover indicates that the level spacing $\Delta E$ is $\sim 40\mu eV$. (b) The crossover from single-level to multilevel transport is also indicated by the change in the proportionality between the width of the peak and T.

## 2.6 Ground State of the Artificial Atom in Strong Magnetic Fields

At zero magnetic field, the energy levels of our single-electron transistor appear to be approximately randomly spaced. This is presumably because the potential in which the electrons are confined is of sufficiently low symmetry that the eigenstates are in the regime of quantum chaos. Predictions have been made for the spacings of levels and their couplings $\Gamma$ to the leads in this regime. However, we have not been able to test these properly so far because the temperature range in which we can probe one level at a time is very small. We expect this to become a major focus of our fundamental physics research on artificial atoms in the next few years when smaller atoms are constructed, for these will have larger level spacings, as discussed below.

At high magnetic fields, the level spacings become more regular. The strong field dominates the motion of the electrons, and only the parabolic component of the confining potential appears to be important. McEuen et al[19] have tried to interpret results in this regime using a constant interaction model: One assumes a constant Coulomb charging energy, $e^2/2C$, for adding each new electron to the atom, and one assumes that once added the electrons do not interact with one another. While this model can explain some of the qualitative features of the experiments, it fails when quantitative comparisons are made.

The next step in modeling the system is to include the electron-electron interaction in a self-consistent but semi-classical (SC) way.[20] This SC model is similar to the Thomas-Fermi approximation and is the kind of modeling usually used for semiconductor devices. Until recently, we thought this was completely satisfactory. However, in the past year we learned how to test the SC model more stringently, and we found that it is also inadequate. One needs to include the exchange interaction between electrons in order to describe the energy spectrum properly. Next, we give a simple physical model that describes the effects of exchange and reviews our recent results.

---

[19] P.L. McEuen, E.B. Foxman, U. Meirav, M.A. Kastner, Y. Meir, N.S. Wingreen, and S.J. Wind, "Transport Spectroscopy of a Coulomb Island in the Quantum Hall Regime," *Phys. Rev. Lett.* 66: 1926 (1991).

[20] P.L. McEuen, E.B. Foxman, J. Kinaret, U. Meirav, M.A. Kastner, N.S. Wingreen, and S.J. Wind, "Self-Consistent Addition Spectrum of a Coulomb Island in the Quantum Hall Regime," *Phys. Rev. B* 45: 11419 (1992).

First, consider the constant interaction model. From calculations[21] as well as infrared studies,[22] we know that the confining potential is approximately parabolic. For non-interacting electrons in a strong magnetic field and a parabolic potential the allowed single particle energies are given by

$$E_i = (n_i+1)\hbar\omega_c + \frac{1}{2} m^*\omega_o^2 l_B^2(m_i+1) + g\mu_B B s_i \quad (8)$$

where $\omega_c = eB/m^*$ is the cyclotron frequency for effective mass $m^*$, $\omega_o$ is the harmonic oscillator frequency from the parabolic confinement potential, $n_i$ is the Landau level (LL) index for electron number i, $l_B$ is the magnetic length defined below, $m_i$ is the quantum number for the z-component of the orbital angular momentum, $\mu_B$ is the Bohr magneton, and $s_i$ is the quantum number for the z-component of the spin angular momentum. The states for a given $n_i$ and $s_i$ can be thought of as orbits with centers at radii $R_i$ given by

$$\pi R_i^2 B = (m_i + 1)\phi_o = (m_i + 1) l_B^2 B, \quad (9)$$

each with an area containing one flux quantum $\phi_o = hc/e$. The total energy of N electrons is found by summing up the single particle energies, given by equation (8) for the ith electron.

The largest term in the energy is $\hbar\omega_c$, so the energies of the higher LLs increase rapidly with increasing magnetic field. At the same time, $l_B$ gets smaller so the confinement (second) term in equation (8) decreases for fixed $m_i$. As a result, electrons fall into successively lower LLs until all electrons are in the lowest LL (n =1). Once this happens, ignoring the Zeeman (last) term in equation (8), the lowest energy sate has all angular momentum states $m_i < N/2$ doubly occupied and all others empty if N is even. If N is odd, there is one unpaired spin in the state with $m_i = N/2 + 1$. The Zeeman term is not really zero so increasing the field further causes electrons with their spin antiparallel to the field (↓) to, one at a time, flip their spins to become parallel to the field (↑). The bare g-value in GaAs is very small ( - 0.44), so the total energy varies very slowly with B for non-interacting electrons once they all are in the lowest LL.

It turns out that the Coulomb interaction is much more important than the bare g-value in causing the spins to flip. As mentioned above, a peak in the conductance occurs when the electrochemical potential of the electron droplet $\mu + \alpha eV_g$ equals that of the leads. Thus, a measurement of the value of $V_g$ at which the Nth peak occurs is equivalent to measuring the chemical potential of the droplet with N electrons. When the magnetic field is increased, $\mu$ varies and displays a jump at fields for which there is a change in the electronic state of the droplet. Recall that the definition of $\mu$ is that it is the derivative of the free energy with respect to particle number. Thus a jump in $\mu$ indicates a change in slope of E vs. N for the ground state (GS), that is, a change in the GS.

Our experiment[23] measures very precisely the magnetic field $B_n$ at which the nth jump in $\mu$ occurs, because at $B_n$ there is a sharp minimum in the peak height. Figure 5 shows the peak position for one peak as a function of B; a few of the peaks as a function of gate voltage are plotted in the inset. The change in behavior near 1.6 T signals the depopulation of all but the lowest orbital LL. We focus on the field regime above this, for which only the lowest orbital LL is occupied. For this region the values of B at which minima occur in the peak height are indicated by arrows. These are the fields at which electrons flip their spins from ↓ to ↑.

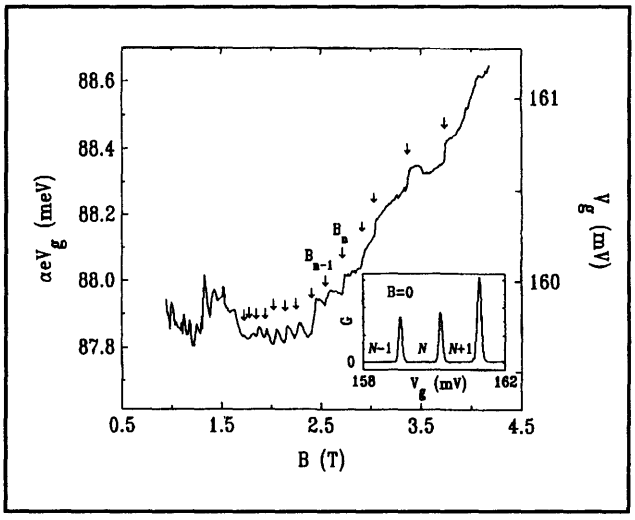


**Figure 5.** Peak position (multiplied by $\alpha e$ to convert to energy) as a function of magnetic field. Inset lower right shows peaks in conductance as a function of $V_g$.

---

[21] A. Kumar, "Self-Consistent Calculations on Confined Electrons in Three-Dimensional Geometries," *Surf. Sci.* 263: 335 (1992).

[22] U. Merkt, "Far-Infrared Spectroscopy of Quantum Dots," *Physica B* 189: 165 (1993).

[23] O. Klein, C. de C. Chamon, D. Tang, D.M. Abusch-Magder, S.-G. Wen, M.A. Kastner, and S.J. Wind, "Exchange Effects in an Artificial Atom at High Magnetic Fields," *Phys. Rev. Lett.*, forthcoming.

By taking differences between the $B_n$, we measure the increase in field necessary to flip one more spin. Therefore, the inverse of the field difference $\chi_n = (B_{n+1} - B_n)^{-1}$ can be thought of as the spin susceptibility of the droplet. Figure 6a shows the results of our measurement of this quantity, plotted versus $B_n$. Figure 6c shows the prediction of the constant interaction model (dashed line) and the SC model.[24] The SC calculation is much superior. The constant interaction model predicts values at least ten times too small and values that increase rather than decrease with B. The SC model predicts values of the correct magnitude which decrease with B, as observed. However, the SC model fails to predict the apparent divergence of $\chi_n$ at the field $B_c$. The SC model includes the electron-electron interaction as well as the Landau quantization, but it ignores exchange.

As seen in figure 6b, Hartree-Fock (HF), which includes exchange, provides a much better description of the data than does the SC model. It predicts the divergence at $B_c$ quantitatively. Fitting the data and the HF calculation to a power law gives the same exponent and the same prefactor, within the errors. This is dramatic evidence that exchange is important in determining the GS of the electron droplet.

To understand why exchange has this effect consider the states that are occupied when there are N↑ up spins and N↓ down spins. The effect of exchange is to reduce the Coulomb repulsion between electrons with parallel spins at small separations. This allows the confinement potential to force the electrons closer together than they would be with the Hartree (long range Coulomb) interaction alone. The result is that all states with $m_i < N\uparrow$ are occupied for spin up and all states with $m_i < N\downarrow$ are occupied for spin down. This gives a very different charge distribution $\rho(r)$ than the SC model. The SC charge density $\rho(r)$ is dome-like except near those values of r where the charge density is close to integer filling fractions $\nu = \phi_o\rho/B$. In these regions, $\rho$ is constant for a range of r because of the incompressibility of the quantum Hall liquid. Sketches of the charge densities for the SC and HF calculations are shown in figure 7.

By summing the single particle energies, one finds that the total confinement energy associated with the HF density is

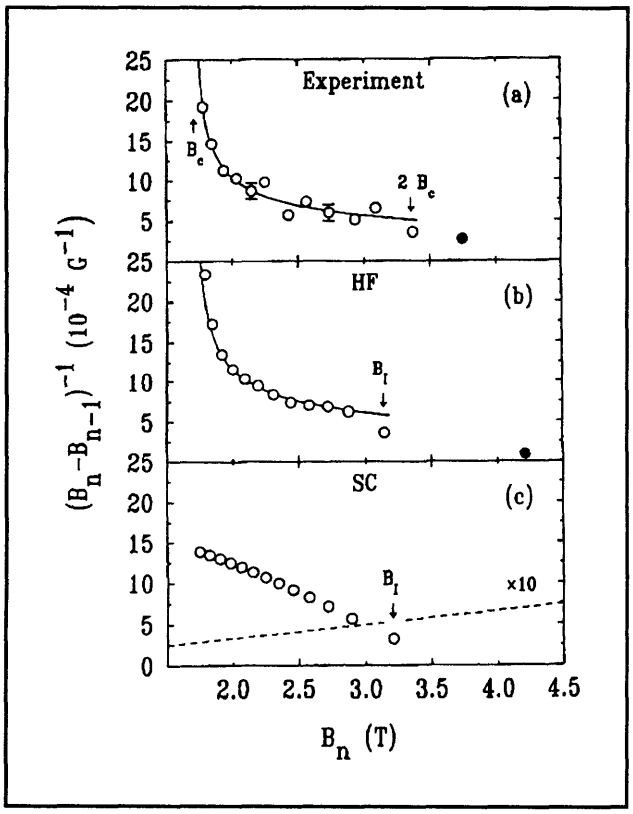


**Figure 6.** (a) Experimental measurement of $\chi_n$. (b) Hartree-Fock calculation of $\chi_n$. (c) Semiclassical (circles) and constant interaction (dashed line) calculations of $\chi_n$.

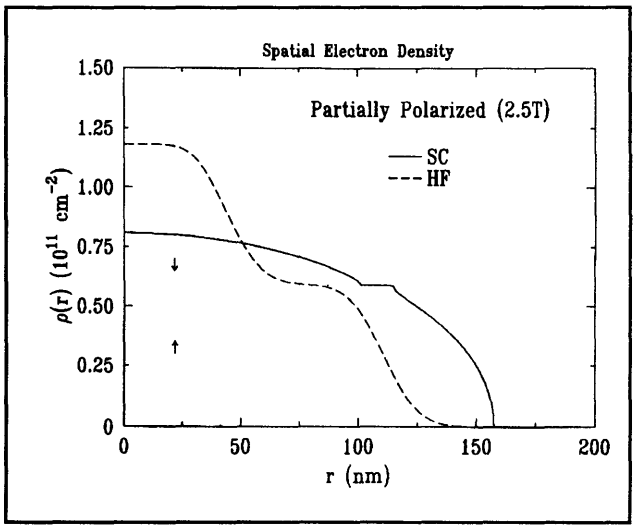


**Figure 7.** Semiclassical (solid line) and Hartree-Fock (dashed line) calculations of the charge density as a function of radius in the droplet. The density corresponding to one flux quantum per electron is shown by a dotted line separating spin down and spin up electrons.

[24] P.L. McEuen, E.B. Foxman, J. Kinaret, U. Meirav, M.A. Kastner, N.S. Wingreen, and S.J. Wind, "Self-Consistent Addition Spectrum of a Coulomb Island in the Quantum Hall Regime," *Phys. Rev. B* 45: 11419 (1992).

$$E_c = \frac{1}{2} m^* \omega_o^2 l_B^2 \{N\uparrow(N\uparrow+1) + N\downarrow(N\downarrow+1)\} =$$

$$\frac{1}{2} m^* \omega_o^2 l_B^2 \{2S^2 + N^2/2 + N\} \qquad (10)$$

where S is the total spin of the droplet $S = (N\uparrow - N\downarrow)/2$. To understand the physics, we treat S as a continuous variable even though it is actually discrete.

The confinement obviously favors the singlet state since $E_c$ is a minimum for S = 0. However, the Coulomb interaction energy among the electrons is largest for the singlet because it has the largest density. We can not write a simple expression for the total Coulomb energy $E_Q$ as we can for $E_c$. However, we know that it is a maximum for S = 0, because the singlet state keeps the electrons as close together as they can be. We also know that an expansion of the Coulomb energy as a polynomial in S will have only even powers because the Coulomb energy must be symmetric if we exchange up for down spins. Thus, the Coulomb energy for small S can be written

$$E_Q = \frac{e^2}{\varepsilon l_B} [c_2 S^2 + c_4 S^4 + ...] + \text{constant} \qquad (11)$$

with the constant $c^2 < 0$. The prefactor $e^2/\varepsilon l_B$ is the obvious scale for Coulomb interactions in a magnetic field because $l_B$ is the distance between successive orbits. Ignoring the Zeeman energy because g is so small, we see that spins flip because, with increasing B at fixed S, $E_c$ decreases as $B^{-1}$ and $E_Q$ increases as $B^{1/2}$ making the confinement less important than the Coulomb repulsion. In fact, were it not for the fourth order term in equation (11), all spins would flip at a single field $B_c$. By considering the balance of $E_C$ and $E_Q$, one predicts that below the field $B_c$ the singlet state is stable, but above $B_c$, the droplet acquires a spin which increases as $(B-B_c)^{1/2}$ or, equivalently, $\chi_n \sim (B-B_c)^{-1/2}$. The exponent we find from the fit of a power law to the data in figure 6a or the HF calculation in figure 6b is 0.4 ± 0.1, within error of the prediction 0.5.

After the droplet is fully polarized at $B_l$, more transitions are observed. These are predicted qualitatively but not quantitatively by Hartree-Fock and probably therefore involve correlations.

## 2.7 Development of Process for Si Single-Electron Transistors

In the past six months, David Abusch-Magder, a graduate student in Physics, has made great progress in developing the fabrication process for single-electron transistors in Si. He has designed a class of devices using a double-gated MOSFET, which he will study to further illuminate both the physical and technological aspects of single electronics. The lower gate, set at a voltage below threshold, keeps most of the p-type surface insulating while the top gate inverts a small open region. The steps in this design were as follows:

**Performed a literature search.** There have been a very limited number of single electron transistors fabricated in silicon MOS systems. There is clearly a lack of knowledge about well controlled single-electron devices in material systems other than metals and GaAs.

**Performed initial simulations to get an idea of the sort of device behavior expected.** We have done initial simulations and have found software that will allow us to do more detailed work as the need arises. We have, however, decided that detailed simulations are less important than actually fabricating devices, and then using simulations as a tool to understand our measurements.

**Designed a silicon process that is simple to carry out and is robust.** We have done this making maximum use of existing technology and experience. Because of our device requirements we have chosen to make the device with a Cr lower metal gate. Since this is non-standard processing it has required additional process development.

**Designed masks.** We have attempted to design our masks to allow for a variety of physical measurements that might be interesting. We have also designed the masks so that a wide variety of lower gate metal patterns can be accommodated. This then allows the exploration of a large device space within the existing mask set and silicon process. We have also designed an optical mask level to pattern the lower metal gate which will allow us to build test devices to assess the impact of the process on the device parameters. Additionally, we have included redundancy in the mask to give a certain amount of fault tolerance.

**Designed and wrote Scanning Electron Beam Lithography (SEBL) patterns on dummy substrates.** Since the nanolithography on this project is very aggressive, it requires significant development work to obtain high quality patterns. We have written hundreds of different patterns at ten different exposure doses to obtain patterns that

will display interesting SET behavior. We have been forced to explore not only exposure and pattern variation, but also surface treatment of wafers, column charging effects, acceleration voltage, resist thickness, liftoff procedure and filament life cycle. Because of this work, we have successfully patterned lower gates with dimensions of 50 nm-100 nm. This is our most unique accomplishment so far.

**Performed initial feasibility studies of our process.** Before processing wafers we tested some key steps that are unique to our process to ensure that a process would be possible. Specifically, we investigated the deposition, patterning, and subsequent processing of our lower gate metal. We performed initial tests to liftoff nanolithographically patterned layers of Cr and trilayers of Cr-W-Cr. We also made sure that Low Temperature Chemical Vapor Deposition (LTCVD) of the oxide between the two gates and the subsequent rapid thermal annealing of these layers did not destroy the conductivity of the lower gate.

**Designed and implemented an alignment scheme.** We require a set of marks that allow both the optical lithography tool as well as the SEBL tool to align the wafer. These respective alignment schemes must be coordinated so all levels of the process are aligned with respect to each other. This had to be done taking subsequent processing into account to ensure that alignment marks do not get "buried".

**Developed detailed process.** This included specifying the process exactly, deciding exactly which machines will be used, and what recipes to follow for every detailed process step. This information then had to be entered into the clean room computerized environment. Several dry runs were necessary to work out minor bugs in the process. This has required significant work by Abusch-Magder in the clean room, both processing wafers and supervising the work of others, to make final decisions about contact hole etching, premetalization cleaning, and top gate metalization.

The following steps are in progress:

**Assess process impact on device parameters.** We are attempting to determine how different processes impact the device parameters. To that end, we have a lot of wafers all with different combinations of doping density, gate oxide thickness, rapid thermal anneal temperature cycle, contact hole etch recipe, and gate metalization. These wafers will then be tested to see how the device parameters vary. Among the device parameters we are examining are oxide charge, high temperature mobility, low temperature mobility, breakdown voltages of the insulating barriers that form on the contacts during processing, and inversion voltage thresholds.

**Process wafers with single-electron devices.** There are currently eight wafers with SEBL patterned lower metal gates that will be processed to completion in the next one to two months.

**Bring device wafers to completion.** This includes dicing and bonding devices. Future processing work includes: Fabricating another round of devices with different lower metal gate patterns to answer unresolved physical questions.

**Finish process development for SEBL patterned wafers at 50 kV.** Our SEBL has so far been done at 25 kV because the parameters at this voltage are known. On the other hand 50 kV gives a smaller spot size so smaller dimensions are possible. We have done initial work at 50 V, but have not finalized a process.

## 2.8 Publications

Foxman, E.B., U. Meirav, P.L. McEuen, M.A. Kastner, O. Klein, P.A. Belk, D.M. Abusch, and S.J. Wind. "Crossover from Single-Level to Multilevel Transport in Artificial Atoms." *Phys. Rev. B.* 50: 14193 (1994).

Klein, O., C. de C. Chamon, D. Tang, D.M. Abusch-Magder, S.-G. Wen, M.A. Kastner, and S.J. Wind. "Exchange Effects in an Artificial Atom at High Magnetic Fields." *Phys. Rev. Lett.* Forthcoming.